

# Enhancement of the SrTiO<sub>3</sub> Surface Reactivity by Exposure to Electric Fields

Kurt Klauke,<sup>[a]</sup> Buğra Kayaalp,<sup>[a]</sup> Mattia Biesuz,<sup>[b]</sup> Alessandro Iannaci,<sup>[c]</sup> Vincenzo M. Sglavo,<sup>[b]</sup> Massimiliano D'Arienzo,<sup>[d]</sup> Siwon Lee,<sup>[e]</sup> Jongsu Seo,<sup>[e]</sup> WooChul Jung,<sup>[e]</sup> and Simone Mascotto<sup>\*[a]</sup>

**Abstract:** In the present work the effect of electric field assisted treatments, i.e. flash sintering, on the physicochemical properties and surface reactivity of SrTiO<sub>3</sub> nanoparticles is investigated. The materials were prepared by a hydrothermal approach and consolidated at high temperatures by conventional and electric field assisted procedures. The exposure to an electric field from 300 to 900 V/cm allowed rapid consolidation with progressive reduction of the grain growth and the shrinkage of the specific surface area to 22% and 43%, respectively. XPS analyses evidenced increasing Sr segregation at the surface if voltage was applied during the treatment. The corresponding presence of Sr vacancies in the

perovskite lattice was demonstrated by ESR spectroscopy. Both techniques pointed out the appearance of highly oxidative O<sup>-</sup> species in all ceramics. The materials reactivity was investigated by methane oxidation, chosen as model high temperature catalytic reaction. With respect to conventionally treated SrTiO<sub>3</sub>, the surface area normalized reaction rate significantly improved for the ceramics exposed to electric field, until a maximum of three times for the material treated at 900 V/cm. Such enhanced properties were ascribed to the larger extent of Sr enrichment and in particular to the correlated field-induced defect structure perturbation.

The preparation of functional materials using field-assisted processes gained increasing attention from the scientific community in the last years. With respect to conventional methods, these strategies notably reduce the reaction time and temperature and are therefore regarded as highly sustainable and environmentally friendly.<sup>[1]</sup> If microwave-assisted syntheses covered a pivotal role in the last decades,<sup>[2–4]</sup> the use of electric and magnetic fields recently emerged as novel strategy towards synthesis and the processing of inorganic materials.<sup>[5]</sup> In addition to the energy-saving character, these methods are very appealing because of i) the possibility to synthesize materials that cannot be prepared by conventional methods,<sup>[6]</sup> ii) the

design of materials with specific microstructure and textures<sup>[7]</sup> and iii) control of defect formation<sup>[8]</sup> and mobility.<sup>[9]</sup>

The consolidation of ceramic materials is an important technological requirement for many high temperature applications such as solid-oxide fuel cells, thermoelectrics and catalysis. In this regards, the pioneering work of Cologna et al.<sup>[10]</sup> on electric-field assisted treatments (i.e. flash sintering) showed that the application of a voltage and current to a ceramic specimen during heating promoted stabilization and consolidation at furnace temperatures far below the conventional ones and within few seconds/minutes. The reason for such a rapid process is principally ascribed to a local overheating of the material via Joule effect.<sup>[11,12]</sup> Hence, it is evident that the electric properties of the ceramics exert a remarkable role on the treatment conditions. Insulating materials such as SrTiO<sub>3</sub> consolidate at furnace temperatures as high as 1000 °C,<sup>[13]</sup> whereas highly conductive systems like La<sub>0.6</sub>Sr<sub>0.4</sub>Co<sub>0.2</sub>Fe<sub>0.8</sub>O<sub>3</sub> well below 100 °C.<sup>[14]</sup>

More importantly, the very intense local heating as a result of the high electric power dissipation through the material has a remarkable effect on the modification of microstructural properties and defect formation.

Karakuscu et al.<sup>[13]</sup> showed that the massive grain growth usually observed in polycrystalline SrTiO<sub>3</sub> under conventional treatment was arrested when the material was treated with the assistance of electric field, and that a direct correlation between applied voltage and grain size exists. Moreover, electric field-treated materials experienced lattice expansion, which was ascribed to the formation of Ruddlesden-Popper phases (SrO (SrTiO<sub>3</sub>)<sub>n</sub>) originating from structural recombination of defect-induced distortions.<sup>[15]</sup> In a more recent publication Rheinheimer et al. showed that the application of an electric field on

[a] K. Klauke, Dr. B. Kayaalp, Prof. Dr. S. Mascotto  
Institut für Anorganische und Angewandte Chemie  
Universität Hamburg  
Martin-Luther-King-Platz 6, 20146 Hamburg, Germany  
E-mail: simone.mascotto@chemie.uni-hamburg.de

[b] Dr. M. Biesuz, Prof. Dr. V. M. Sglavo  
Dipartimento di Ingegneria Industriale  
Università degli Studi di Trento  
Via Sommarive 9, 38123 Trento, Italy

[c] Dr. A. Iannaci  
INSTM  
Trento Research Unit  
Via G. Giusti 9, 501211 Florence, Italy

[d] Prof. Dr. M. D'Arienzo  
Dipartimento di Scienze dei Materiali  
Università di Milano-Bicocca  
Via R. Cozzi, 55, 20125 Milano, Italy

[e] S. Lee, J. Seo, Prof. Dr. W. Jung  
Department of Materials Science and Engineering  
Korea Advanced Institute of Science and Technology  
291 Daehak-ro, Yuseong-gu, Daejeon 34141, Republic of Korea

 Supporting information for this article is available on the WWW under <https://doi.org/10.1002/cnma.201900201>

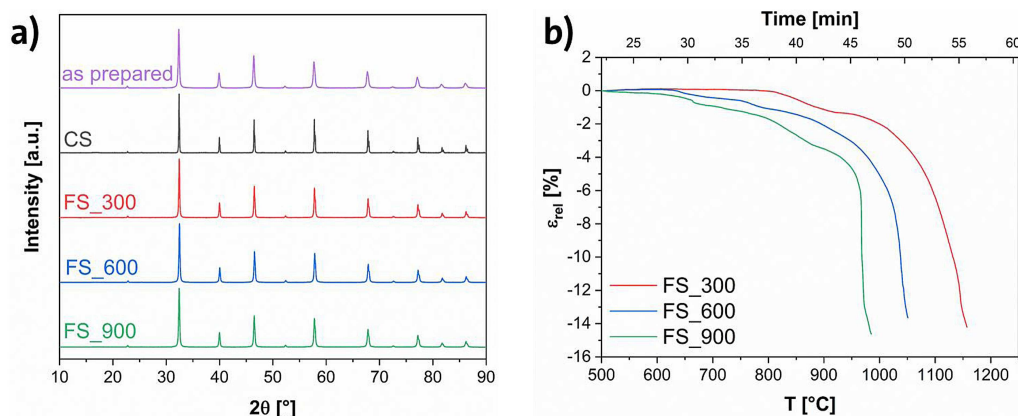


**Figure 1.** (a) X-ray diffraction patterns of the as prepared and high temperature treated SrTiO<sub>3</sub>. (b) Plots of the linear shrinkage against the furnace temperature during the electric field assisted treatment.

SrTiO<sub>3</sub> caused point defect redistribution, affecting the space charge potential at the grain boundaries.<sup>[9]</sup>

Hence, along with this prominent manipulation of structural and defect properties, the electric field-processed materials should demonstrate substantial reactivity difference with respect to conventional counterparts. However, to the best of our knowledge these aspects are not addressed within the existing literature. In the present publication, we show that electric field-treated SrTiO<sub>3</sub> nanoparticles possess improved catalytic activity with respect to conventional systems due to their larger point defect concentration. SrTiO<sub>3</sub> was chosen primarily because it is a model material with well-known defect chemistry, rather than for its catalytic activity. As chemical purity and morphology homogeneity were considered of central importance, ceramic nanoparticles were prepared by means of the hydrothermal method.<sup>[16]</sup> For the evaluation of the material reactivity the total methane oxidation was employed as typical high-temperature test reaction.

In general, in a catalytic reaction over perovskite oxides (ABO<sub>3</sub>) the material reactivity is determined both by the overlap extent between the 3d orbitals of the B cation and the 2p of the oxygen<sup>[17]</sup> as well as by the surface activity of the material, which can be affected by an enrichment of the A-type cation through a segregation process at high temperature. Because of the unoccupied e<sub>g</sub> orbitals Ti is a poor catalytic center for the methane oxidation and therefore its reactivity is mostly controlled by the surface properties. Recently, several reports pointed out how specific modification of the surface morphology and surface chemistry of SrTiO<sub>3</sub> engendered strong alteration of its catalytic properties.<sup>[18–21]</sup> Herein we show how the exposure to electric fields enhances the amount of Sr surface enrichment and this determines a progressive improvement of the methane conversion. Even though the segregation of Sr is usually indicated as one major factor for the performance loss of catalytic devices, in certain cases it was shown to improve the material reactivity.<sup>[18,22,23]</sup> In particular, it has been reported that Sr surface segregation has a beneficial effect towards methane oxidation.<sup>[24,25]</sup> Hence, aside from their energy-saving character, field-assisted treatments can be con-

sidered as a valuable tool to tune the surface chemistry of ceramic materials and therefore to improve their catalytic performance.

## Results and Discussion

Strontium titanate nanoparticles were prepared via the hydrothermal approach. XRD analysis evidenced phase pure cubic perovskite structure, with average crystal size of 50 nm (Figure 1, Table 1). In Figure 3a and Figure S1a the electron micro-

**Table 1.** Physicochemical parameters for the investigated SrTiO<sub>3</sub> systems: Crystallite size (Φ); specific surface areas (S<sub>BET</sub>); Sr/Ti ratio; ratio between non-lattice Sr (Sr<sub>NL</sub>) and total Sr amount (Sr<sub>TOT</sub>) and surface concentration of O<sub>2</sub><sup>2-</sup>/O<sup>-</sup> obtained from XPS; surface area normalized activation energies (E<sub>a</sub><sup>cat</sup>) values retrieved from methane oxidation. \*Obtained from TEM/EDX spectroscopy.

Sample	Φ [nm]	S <sub>BET</sub> [m <sup>2</sup> g <sup>-1</sup> ]	Sr/Ti	Sr <sub>NL</sub> /Sr <sub>TOT</sub> [%]	O <sub>2</sub> <sup>2-</sup> /O <sup>-</sup> [%]	E <sub>a</sub> <sup>cat</sup> [kJmol <sup>-1</sup> ]
CS	> 200	12.7	1.34/ 1.12*	7	10.6	136.1
FS_300	110	6.0	1.4	32.2	11.4	136.5
FS_600	80	9.4	1.45/ 1.17*	39.8	6	131.7
FS_900	70	11.9	1.55	39.1	10	120.0
AP	50	27.4	1.02*	–	–	–

scopy showed nanocuboids of dimensions ranging between 50 and 100 nm and the associated energy dispersive X-ray (EDX) spectroscopy analysis indicated stoichiometric amounts of Sr and Ti.

The materials were therefore consolidated via high temperature treatment (HTT) using conventional and electric field-assisted process (Figure 2).

This trend is also corroborated by SEM analysis (Figure 3b–e), which clearly evidenced the particle growth arrestment during electric field-assisted treatment and the massive size of the standardly treated ceramic.

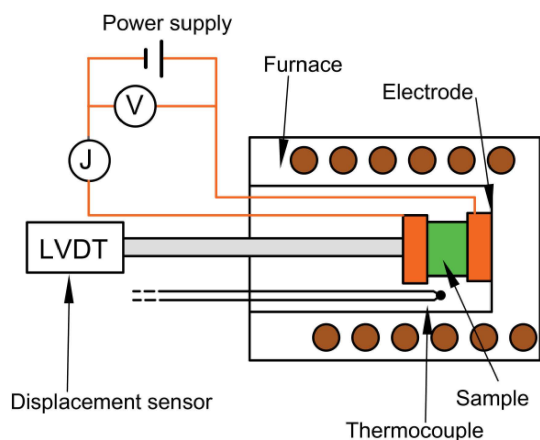


**Figure 2.** Schematic representation of the setup for the electric field assisted treatments.

The porosity of the SrTiO<sub>3</sub> samples was investigated by means of gas physisorption. Even though the materials present the same density of 60%, the specific surface area strongly decreased upon HTT. For the electric field treated samples this shrinkage was moderate and indirectly proportional to the magnitude of the applied field, in line with the material grain evolution (Table 1). CS material however, exhibited a BET surface area much higher than FS\_300 material and comparable to FS\_900. A reason for this behavior is likely the different temperature program, which might have induced a different structural reorganization of the material. The high porosity of the electric field treated materials was further evidenced by TEM analysis taken from a section of the FS\_600 pellet (Figure 3f).

Making use of the X-ray photoelectron spectroscopy (Figure S2), major insights into the local variation of the surface

chemical composition depending on the HTT could be given. The spectra of all the materials reveal higher surface content of strontium than titanium (Table 1). A precise analysis of the Sr3d spectra revealed that the contribution of the non-lattice Sr, increases under exposure to electric field (Figure 4a, Figure S3, Table 1). Although the amount of non-lattice Sr is also directly related with the porosity of the material, we observed that for the conventionally treated sample, that is the one with highest surface area, this value is much lower than for the other materials. Hence, we can conclude that the Sr enrichment observed is an intrinsic consequence of the electric field assisted treatment and is not related with the morphological properties of the single ceramics. From the chemical point of view, non-lattice Sr can be related to the formation on the surface of Sr(OH)<sub>2</sub>, SrCO<sub>3</sub>, under-coordinated Sr cations or a combination of these three and gives an indication of the extent of Sr surface segregation.

XPS results were also confirmed by TEM/EDX analyses (Table 1, Figure S1b,c). Given the higher penetration depths of EDX, these findings indicate that the electric field-induced Sr segregation is not limited to few nanometers, but has a more bulk character.

This enrichment phenomenon is usually encountered in high temperature treated SrTiO<sub>3</sub>. Even if there are numerous reactions, which could lead to Sr segregation, one possible explanation is given by the material defect equilibrium<sup>[29–31]</sup> in the Kröger-Vink notation (Eq.1).<sup>[32]</sup>



During high temperature treatments ( $T \geq 1000^\circ\text{C}$ ) Sr and O ions leave their lattice positions ( $Sr_{sr}$ ,  $O_o$  respectively) and Sr- ( $V'_{sr}$ ) and O-vacancies ( $V_o^{2*}$ ) are formed. The formation of Ti-vacancies does not take place as it requires much higher energy because of the higher covalent character of the Ti–O bond.<sup>[33,34]</sup>

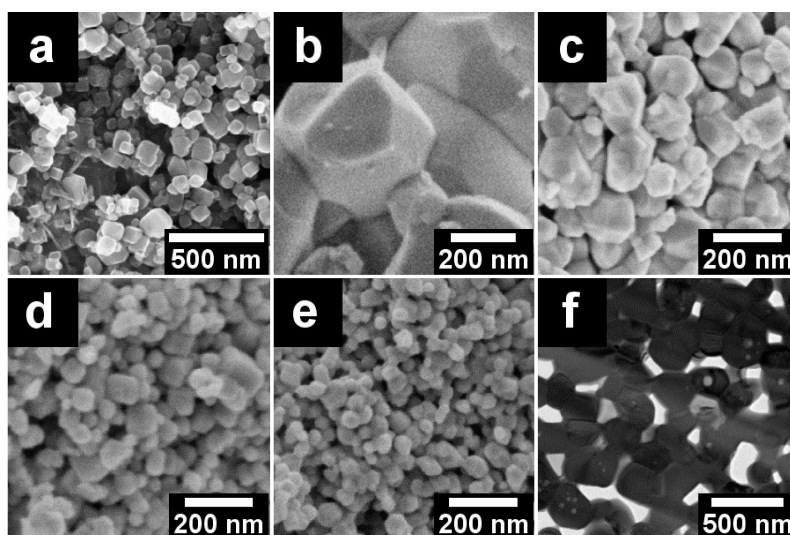


**Figure 3.** SEM images of (a) as prepared nanoparticles, (b) conventionally treated sample (CS), (c, d, e) samples treated under the exposure of 300, 600 and 900 V/cm, respectively; (f) TEM image of a lamella cut from sample FS\_600 with a focused ion beam, showing the porous structure of the materials.

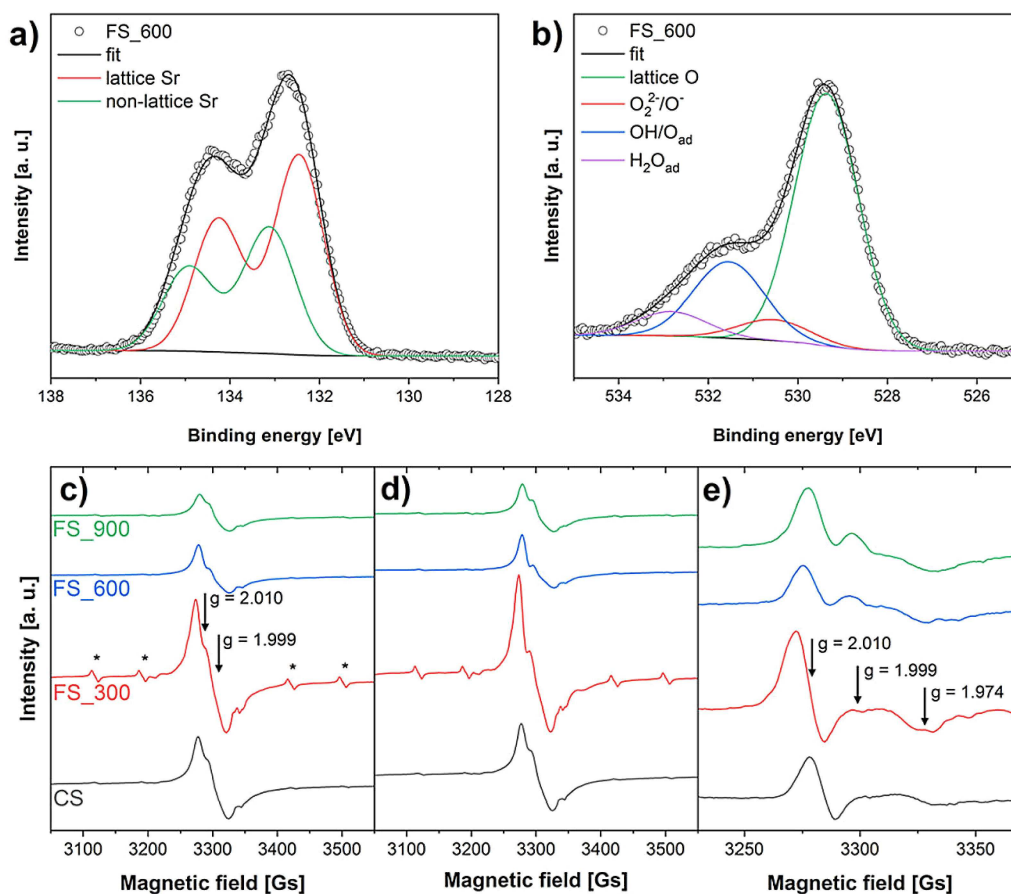


**Figure 4.** (a) Sr3d spectrum of FS\_600 evidencing the two components of lattice and non-lattice Sr; (b) O1s spectrum of FS\_600 exhibiting the different oxygen species at the surface. ESR spectra of SrTiO<sub>3</sub> powders at 130 K in vacuum (c) before and (d) after UV photoexcitation. (e) Spectral features of the most relevant paramagnetic species obtained by subtracting the spectra of UV-irradiated samples from the spectra acquired before irradiation.

As a result of the mass conservation law, a separate phase of SrO (ideally noted as one of manifold possibilities) is formed at the grain surface and interface.<sup>[31]</sup> In the case of the electric field-treated materials, the origin of the extent of Sr enrichment at the surface is not completely clear yet. It might originate from the localized thermal gradient at the microstructural level. As shown elsewhere, during electric field-assisted consolidation of insulating materials local overheating<sup>[28]</sup> or even melting<sup>[35]</sup> of the grain boundaries occurs. Thus, such temperature gradients in the grain might cause defect redistribution and contribute to explain the larger Sr segregation. However, an interaction between the electric field/current and the defect chemistry cannot be ruled out. As a matter of fact, field-induced defect perturbation has been often proposed as the pivotal mechanism for field-assisted sintering of ceramics.<sup>[28,36,37]</sup>

The O1s signal was deconvoluted taking into account four different oxygen species (Figure 4b, Figure S4): the lattice oxygen (O<sup>2-</sup> at ~529.2 eV), highly oxidative oxygen species (O<sup>-</sup>/O<sub>2</sub><sup>2-</sup> at ~530.5 eV), hydroxyl groups or adsorbed oxygen (OH/O<sub>2</sub> at ~531.5 eV) and adsorbed water (H<sub>2</sub>O at ~532.9 eV).<sup>[38]</sup> Several reports in the literature correlate the oxidative O<sup>-</sup>/O<sub>2</sub><sup>2-</sup> centers to the presence of surface oxygen and strontium vacancies, and therefore strongly related to the defect species listed in

Eq. 1.<sup>[38–40]</sup> However, we found that the amount of oxidative oxygen is slightly higher for the system treated at 300 V/cm, but generally does not vary much depending by the type of material (Table 1).

Considering the paramagnetic character of the O<sup>-</sup> centers, further investigations were performed by means of electronic spin resonance spectroscopy (Figure 4c–e). All the samples display a complex spectrum constituted by two main resonance lines, which have been assigned to different defect centers (Figure 4c). In detail, the sharp signal at  $g = 2.010$  may be associated to oxygen-related species, i.e. O<sup>-</sup> anions.<sup>[41–43]</sup> The other superimposed signal at  $g = 1.999$  is on contrast not easy to assign. According to Kutty T.R.N et al.,<sup>[42]</sup> the formation of O<sup>-</sup> centers can be correlated with the presence of strontium vacancies located in the proximity of the subsurface region. Based on this consideration, they attributed the resonance at  $g = 1.999$  to singly ionized strontium vacancies ( $V_{Sr}'$ ), which are generally stabilized via HTT. However, the origin of this signal is still controversial. In an attempt to provide a fair attribution of the overlapping signals at  $g \sim 2$  occurring in SrTiO<sub>3</sub> materials, their behavior under UV photoexcitation has been studied. For all the samples, the spectra show a remarkable increase of the intensity of the signal at  $g = 2.010$ , while that at  $g = 1.999$  seems

almost unaffected by the UV irradiation (Figure 4d). The trend is highlighted in Figure 4e, which illustrates the spectral features of the most relevant paramagnetic species in SrTiO<sub>3</sub> obtained by subtracting the spectra of UV-irradiated samples from those acquired before irradiation.

These results suggest that the sharp signal at  $g=2.010$  can be effectively associated to O<sup>-</sup> acceptor centers located close to the valence band and probably connected to the presence of Sr vacancies generated during the HTT. The associated disruption of the chemical bonds with O<sup>2-</sup>, perturb the filled valence band of SrTiO<sub>3</sub> made up of 2p oxygen orbitals. The intensity of O<sup>-</sup> species either before or after photoexcitation appears higher in FS<sub>300</sub> compared to the other materials. Such results are complementary and in very good agreement with the XPS measurements.

Finally, other minor features can be detected, especially in the 300 V/cm treated material. Besides a weak signal at  $g=1.974$  attributable to Ti<sup>3+</sup> species (or, more descriptively, Ti<sup>3+</sup>-V<sub>O</sub>-Ti<sup>4+</sup>, i.e. an electron captured at the oxygen vacancy in the perovskite structure which is delocalized between two Ti<sup>4+</sup> cations), the presence of small Mn<sup>2+</sup> defects (signals labeled with \*) is noticed with  $g$ -value and hyperfine constant of 2.0036 and 85 G, respectively. These impurities usually detectable in even in pure SrTiO<sub>3</sub> systems derive from manganese substitution for titanium ions<sup>[44]</sup> and could explain the higher concentration of O<sup>-</sup> species in FS<sub>300</sub>.

Insights into the transport behavior of the defect species in the HTT materials were obtained by EIS measurements. In the intermediate temperature regime (400–700 °C) and under oxidizing conditions the conductivity of SrTiO<sub>3</sub> is determined by two principal charge carriers: electron holes and oxygen vacancies.<sup>[45,46]</sup> Electrons and strontium vacancies under these conditions are of negligible amount and not sufficiently mobile, respectively. As the mobility of the ionic species is much lower than that of holes, the conductivity is predominantly electronic. For the conventionally treated material a linear variation of the conductivity as function of the oxygen partial pressure with slope of 0.25 is observed (Figure 5).<sup>[45]</sup> Lower conductivities associated with a reduction of the curve slope are registered for the field assisted-treatments. This phenomenon is ascribed to the particle size reduction of the materials, as already observed.<sup>[47–49]</sup> From the Arrhenius plot of the conductivity, the activation energy for charge migration values was determined to be approx. 1 eV for all consolidated materials (Figure S5), independent of the oxygen partial pressure applied and in line with literature values.<sup>[48]</sup>

At this point it is necessary to evaluate whether the drastic changes in the physicochemical properties of the materials exposed to the electric field have influence on their functional properties. With this respect, we investigated the full oxidation of methane as high temperature model catalytic test. In Figure 6a the light-off curves of the methane oxidation over the consolidated materials are shown. At 800 °C conventionally treated SrTiO<sub>3</sub> shows a conversion of 20% whereas for electric field-treated systems the performances progressively increase proportionally with the applied field, up to 33% for SrTiO<sub>3</sub> exposed to 900 V/cm. The gradual increase in catalytic activity

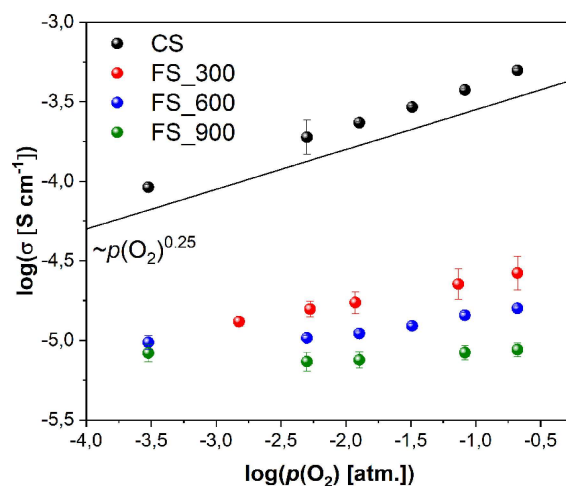


Figure 5. Logarithmic plot of the specific conductivity against the oxygen partial pressure. A slope of 0.25 is obtained for SrTiO<sub>3</sub> single crystal.

depending on the applied field can be caused by the difference of the total specific surface area, because the reactivity per gram of sample is highly proportional to the specific surface area of the sample (Figure S6). In order to obtain a clear understanding of the catalytic activity, the data need to be normalized by the total specific surface area as this parameter changes significantly with respect to the treatment adopted.

From the surface-area-normalized reaction rates at 700 °C in Figure 6 < xfig6 < b, it is clear that the exposure to high electric fields increases the catalytic activity by a maximum of 3 times with respect to the conventionally treated material. Further evidence of the beneficial effect of the electric field is given by the constant decrease of the activation energy of the methane oxidation (Table 1 and Figure S6) by incremental voltage. The E<sub>a</sub> values were calculated from Arrhenius type plots (1,000/T vs. reaction rate) and obtained below 10% conversion of methane.

Interestingly, the catalytic properties were maintained or even improved after 6 months ageing for all the materials treated under influence of the electric field (Figure S7). This indicates an excellent catalytic stability, likely caused by a permanent perturbation of the defect structure by the field exposure.

As XPS analysis showed, also Sr segregation increased with the exposure to the electric field. In principle it is counter-intuitive to assess that Sr surface enrichment promotes the catalytic reaction, because carbonates, oxide or hydroxide species act as a blocking layer hindering the oxygen exchange kinetics and the access of the gas molecules to the catalytic centers.<sup>[50,51]</sup> However, it has been shown often that Sr segregation improves the catalytic performances in perovskites.<sup>[18,22,23,52–54]</sup> Polo-Garzon et al. showed that Sr-enrichment on SrTiO<sub>3</sub> increased the oxidation of 2-propanol to acetone.<sup>[18]</sup> This phenomenon was ascribed to the larger basic character of Sr-terminated surfaces, which improved the dehydrogenation capability of the material. Similar reports on the methane oxidation over surface modified SrTiO<sub>3</sub> pointed out that the surface concentration of Sr at the top layers is

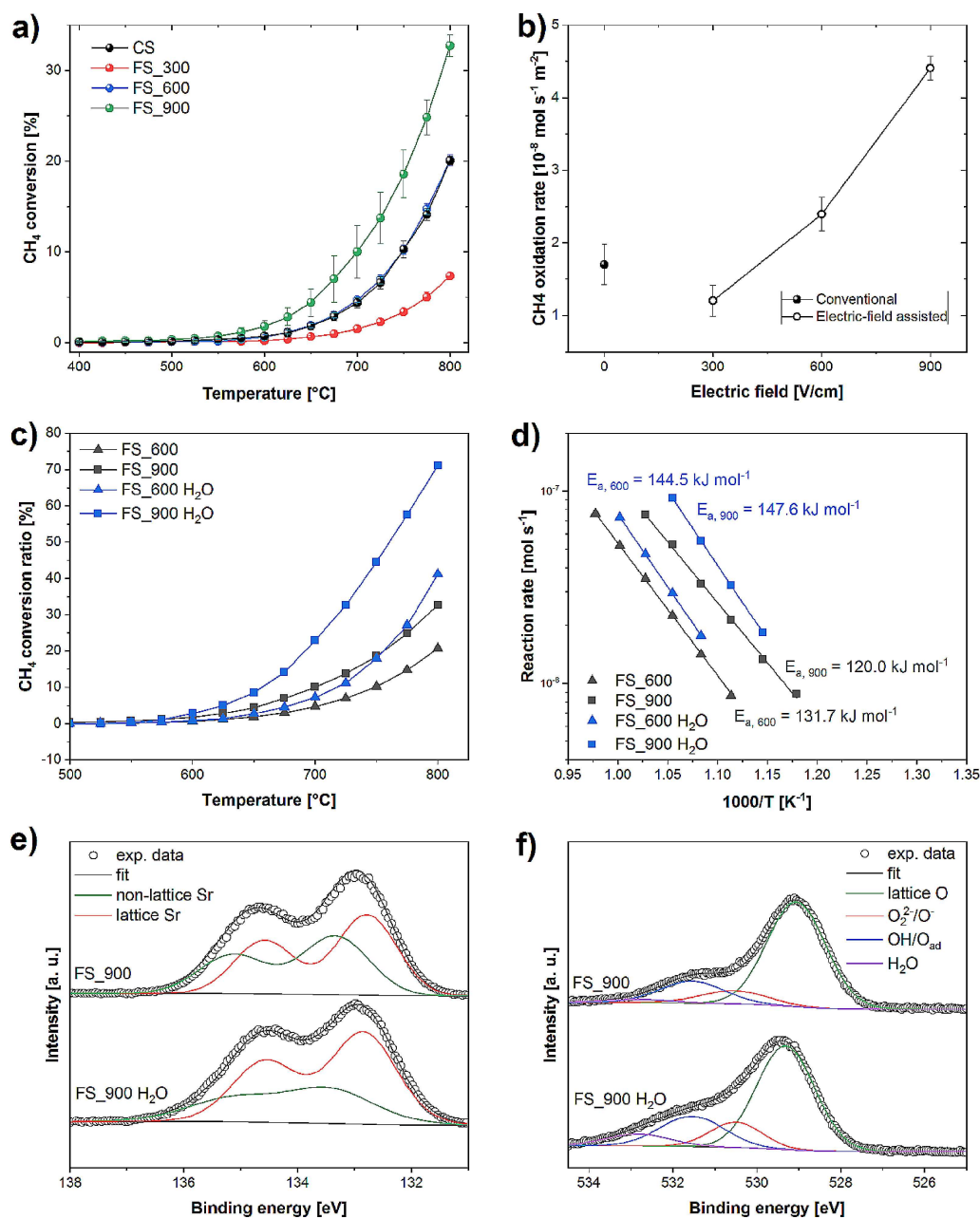


**Figure 6.** (a) Light-off curves obtained from the methane oxidation experiments. (b) Reaction rates at 700 °C normalized by the BET surface area. (c) Light-off curves and Arrhenius plots of the reaction rate (d) of FS<sub>600</sub> and FS<sub>900</sub> samples before (grey) and after (blue) hot water treatment. Sr3d (e) and O1s (f) XPS spectra of SrTiO<sub>3</sub> exposed at 900 V/cm before (FS<sub>900</sub>) and after (FS<sub>900</sub> H<sub>2</sub>O) hot water treatment.

proportional to the rate of methane combustion.<sup>[24,25]</sup> La<sub>1-x</sub>Sr<sub>x</sub>MnO<sub>3</sub><sup>[54]</sup> and La<sub>0.6</sub>Sr<sub>0.4</sub>Co<sub>0.8</sub>Fe<sub>0.2</sub>O<sub>3-δ</sub><sup>[53]</sup> exhibited significant Sr enrichment and the formation of novel compositions at the surface, when exposed to an electric field at high temperatures. These works showed that these surface phases are activated, possessed improved surface exchange kinetics and therefore an enhanced electrocatalytic performance.<sup>[53]</sup> As proposed by Li et al.,<sup>[52]</sup> in the first stage of Sr segregation, when no dense SrO layer has formed yet, the cationic enrichment leads to the formation of oxygen vacancies and to a change of the electronic structure, resulting in a reactivity improvement of the

material. If strontium ions in SrTiO<sub>3</sub> migrate towards the surface forming different phases, it is evident that the corresponding vacancies are left behind (see ESR analysis above) and the perovskite lattice can be considered as A-site deficient. A-site deficiency promotes the oxygen exchange kinetics and therefore has beneficial effect for the catalytic properties of perovskite oxides.<sup>[55-57]</sup> In particular, improved catalytic activity has been recently shown when highly oxidative oxygen (O<sub>2</sub><sup>2-</sup>/O<sup>-</sup>) is present in A-site deficient perovskites, as a result of surface oxygen vacancies.<sup>[38]</sup> In another work,<sup>[42]</sup> the presence of

such hole centers close to the surface was found to be stabilized by Sr vacancies, because they act as acceptor species.

In order to identify whether the improved catalytic properties were determined by the higher basicity of the Sr-enriched surface or by the presence of oxygen defects originated by the modified point defect structure of field-exposed ceramics, we performed additional catalysis experiments after decrease of the surface Sr excess by treatments with water at 80 °C for 3 h.

From the light off curves of the water treated FS\_600 and FS\_900 materials in Figure 6c a significant enhancement of the methane conversion is detected, along with a slight increase of the activation energy of the reaction (Figure 6d). XPS analyses of the Sr3d (Figure 6e, Table S1) confirmed the decrease of the surface Sr-segregation, as noted by the lower contribution of the non-lattice species. Therefore, the reason of the improved performance of the materials cannot be mainly ascribed to the basicity of the SrTiO<sub>3</sub> surface, but other effects need to be taken into account. Surface analysis of the oxygen species (Figure 6f, Table S1) pointed out that the contribution of the hydroxyl groups and oxidative oxygen increased after treatment with hot water.

In particular, O<sub>2</sub><sup>2-</sup>/O<sup>-</sup> species cover an important role in the oxidation mechanism of methane, because they readily react with it to form methoxide, which accelerates the dissociative adsorption and methane dehydrogenation.<sup>[58–62]</sup> Therefore, we can conclude that the presence of such hole centers on the surface, likely stabilized by the defective structure of field-treated materials, can be ascribed as major responsible for the catalytic conversion of methane over SrTiO<sub>3</sub>.

## Conclusion

In the present work we investigated the effect of electric fields during high temperature treatment on the physicochemical and catalytic properties of SrTiO<sub>3</sub> nanoparticles. We observed that the exposure at high electric fields from 300 to 900 V/cm progressively arrested the grain growth and the porosity shrinkage along with a consequent drop of the electrical conductivity. With respect to the materials composition, XPS analyses pointed out the presence of highly oxidative oxygen species O<sub>2</sub><sup>2-</sup>/O<sup>-</sup> in all the systems, whereas an increasing segregation of Sr at the surface arose if voltage was applied during the treatment. ESR spectroscopy confirmed the appearance of the paramagnetic oxygen species along with the one of Sr vacancies in the perovskite lattice. The materials reactivity was probed by methane oxidation, used as catalytic test reaction. With respect to conventionally treated SrTiO<sub>3</sub> the catalytic activity constantly improved for the ceramics exposed to the electric field, until a maximum of three times in the material treated at 900 V/cm. The reason for such enhanced properties was ascribed to the larger extent of Sr segregation and particularly to the correlated modification of the surface oxygen defects. Therefore, although the specific mechanism is not yet completely elucidated, it is concluded that electric field assisted treatments affect the catalytic reactivity of the oxide surface and that the structural and defect properties modified

by the electric field play a role. Through the precise tuning of the surface chemistry properties, this approach offers promising perspectives to design functional ceramics with tailored catalytic properties.

## Experimental Section

### Chemicals

Strontium acetate hemihydrate (98%, Sr(OOCCH<sub>3</sub>)<sub>2</sub>·0.5H<sub>2</sub>O) and titanium (IV) isopropoxide (97 + %, Ti[OCH(CH<sub>3</sub>)<sub>2</sub>]<sub>4</sub>) were purchased from Alfa Aesar. Ethanol (99.9%, C<sub>2</sub>H<sub>6</sub>O) was purchased from VWR Chemicals. Glacial acetic acid (C<sub>2</sub>H<sub>4</sub>O<sub>2</sub>) was purchased from Fisher Chemicals. Sodium hydroxide (98.5%, NaOH) was purchased from Acros Organics. All chemicals were used as received without further purification.

### Preparation of SrTiO<sub>3</sub> Nanoparticles

SrTiO<sub>3</sub> nanocuboids were prepared via a modified hydrothermal synthesis route adapted from ref.<sup>[26]</sup> In a typical synthesis 10.0 mmol of titanium (IV) isopropoxide were dissolved in 30.0 mL ethanol. A second solution containing 10.0 mmol of strontium acetate hemihydrate dissolved in 20.0 mL glacial acetic acid was slowly added to the first solution. The resulting sol was stirred for 1 h at room temperature.

Subsequently, the solvents were evaporated under continuous stirring at 75 °C. The obtained solid was ground to a colorless powder. 0.7 g of the powder was placed into a 10 ml Teflon-liner and a 2 M NaOH solution was added up to 80% of the liner's total volume. The Teflon-lined stainless steel autoclave was placed in an oven under autogeneous pressure for 24 h at 170 °C and then allowed to cool down. The SrTiO<sub>3</sub> precipitate was washed thoroughly with deionized water and dried at 80 °C overnight.

### High Temperature Treatments

Cylindrical pellets with a diameter of 8 mm and a thickness of roughly 3 mm were prepared by uniaxial pressing at 350 MPa. The two flat sides of the green components were painted using a carbon-based conductive cement (Plano GmbH) and then subjected to flash consolidation. The process was carried out in a modified dilatometer (Linseis L75) using a heating rate of 20 °C min<sup>-1</sup>. The samples were placed between two platinum disks connected to a DC power supply (Glassman EW 5 kV, 120 mA) and a multimeter (Keithley 2100). Current, voltage, the furnace temperature and the displacement of the dilatometric piston were recorded at 1 Hz. The field-assisted sintering experiments were carried out using electric fields of 300 V/cm, 600 V/cm and 900 V/cm and a current limit of 2.5 mA/mm<sup>2</sup>; upon reaching the current limit, the current was held at 2.5 mA/mm<sup>2</sup> for 30 s, then the power supply and the dilatometer furnace were switched off. Conventionally sintered (CS) bodies were also manufactured following two different firing schedules: (i) the same cycle of the flash process (20 °C/min) up to the flash temperature, (ii) from room temperature to 900 °C at 5 °C /min, from 900 °C to 1050 °C at 0.5 °C/min, dwelling at 1050 °C for 4 h.

The bulk density ( $\rho$ ) of the samples was measured geometrically. The relative density of the samples was obtained using a value of 5.12 g/cm<sup>3</sup> for fully dense SrTiO<sub>3</sub>.

Samples were labelled as follows: as prepared SrTiO<sub>3</sub> (AP); conventionally treated SrTiO<sub>3</sub> (CS); SrTiO<sub>3</sub> treated with the assistance of

electric field ( $FS_x$ ), where  $x=300, 600$  or  $900$ , depending by the magnitude of the field.

### Impedance Spectroscopy

Impedance measurements were performed using a Novocontrol Alpha A impedance analyzer connected to a NorECs Probostat® sample chamber. A Novocontrol-HT controller connected to a type S thermocouple mounted next to the sample was employed for temperature control. Frequencies in the range of  $10^{-2}$  Hz to  $10^7$  Hz were employed with an amplitude of  $100\text{ mV}_{\text{rms}}$  for all measurements. Novocontrol WinFIT was used for data evaluation and equivalent circuit fitting. An equivalent circuit consisting of three RQ elements usually ascribed to grain boundary, bulk and electrode interface contributions was employed to fit the experimental data. The total resistivity was obtained from the resistances corresponding to the two high frequency arcs in the Nyquist plot. Due to the porous structure of the samples and the insufficient difference in time constants no further analysis regarding grain boundary and bulk contributions was carried out. The oxygen partial pressure was set by mixing Ar 5.0 with air using MKS MF-1 mass flow controllers. Partial pressures were monitored using a NorECs miniature oxygen sensor electrode with a sealed internal metal/metal oxide reference and a Rigol DM-3058 multimeter.

A constant gas flow of 19 sccm was employed for all measurements with the gas supply tube ending in close proximity to the sample. All samples were equilibrated for 13 hours at  $600^\circ\text{C}$  and the desired partial pressure. Each temperature was held for 3 hours before a measurement was performed.

### Electron Microscopy

Scanning electron microscopy (SEM) images were obtained on a LEO1550 with a spatial resolution of  $\approx 1\text{ nm}$ . The powder was fixed on a standard carbon conductive tab and was investigated without further conductive coating.

Transmission electron microscopy (TEM) measurements were carried out on a JEOL JEM 2200 FS at 200 kV equipped with two CEOS Cs correctors (CETCOR, CESCOR), a Gatan 4 K UltraScan 1000 camera and a HAADF (high angle annular dark field) detector. The sample was crushed into a fine powder, which was suspended in toluene by sonication and dropped on a carbon coated 400 mesh TEM grid. The excess of solvent was removed with a filter paper and by drying the grid under air.

Energy dispersive X-ray (EDX) mapping was implemented on several analysis points on the particle and average atomic ratios were calculated for each cation in the perovskite oxides. Analyses were repeated at least on three positions for each sample and less than 1.0 at.% disparity was observed for surveyed cations at each point.

### Gas Physisorption

Nitrogen physisorption isotherms were obtained at  $77.4\text{ K}$  using a Quadrasorb SI-MP by Quantachrome. Outgassing was performed with a Masterprep Degasser (Quantachrome Corp.) at  $120^\circ\text{C}$  for 12 h. Specific surface areas were determined with the Brunauer-Emmett-Teller (BET) method<sup>[27]</sup> at relative pressures  $p/p_0=0.07-0.3$ . The occupation area of nitrogen was assumed to be  $16.2\text{ \AA}^2$ .

### X-ray Photoelectron Spectroscopy (XPS)

X-ray photoelectron spectroscopy was performed using a Sigma probe (Thermo Scientific, USA) under ultrahigh vacuum environment with a  $400\text{ }\mu\text{m}$ -diameter beam of monochromatic X-ray source, Al K $\alpha$  ( $h\nu=1486.6\text{ eV}$ ) radiation. High-resolution XPS scans of oxygen 1s and strontium 3d were carried out to obtain detailed information on these species.

### Electron Paramagnetic Resonance (ESR)

The Electron Spin Resonance (ESR) investigation on SrTiO<sub>3</sub> (STO) samples was performed by using a Bruker EMX spectrometer operating at the X-band frequency and equipped with an Oxford cryostat working in the temperature range of 4–298 K. The nanocrystals were charged in quartz glass tubes connected both to a high-vacuum pumping system. Spectra were recorded under in vacuo conditions ( $10^{-5}$  mbar) at 130 K, before and after 30 min of UV irradiation (UV 150 W Xe lamp, Oriel with the output radiation focused on the samples in the cavity by an optical fiber) in vacuo at the same temperature.

### Catalysis Tests

The catalytic tests were conducted at atmospheric pressure with a fixed-bed flow quartz reactor having an internal diameter of 4 mm. Quartz wool was initially loaded in the middle of the reactor. Then, 100 mg of the catalyst mixed with 200 mg of quartz sand were loaded between 100 mg of quartz sand layers on each end. The temperature of the catalyst was measured using a K-type thermocouple which was in contact with the catalytic bed (Figure S8 and Figure S9). To investigate the effect of hot water treatment on catalytic activity of methane oxidation, we put FS-STO samples into 15 mL of D.I. water which is maintained at  $80^\circ\text{C}$ , and stirred samples at 500 rpm for 3 hours. The feed of methane oxidation (composed of 2 vol% CH<sub>4</sub>, 4 vol% O<sub>2</sub> in Ar balance) was flowed into the reaction. The total flow rate was adjusted for methane oxidation to  $50\text{ mL min}^{-1}$  corresponding to weight hourly space velocity (WHSV) of  $30,000\text{ mLg}^{-1}\text{h}^{-1}$ . The reactant and product gases were monitored using a quadrupole mass spectrometer (Pfeiffer Vacuum GSD320) in real time. The light-off curve was measured with a ramping rate at  $3^\circ\text{C min}^{-1}$ , after activating the catalysts in the reaction atmosphere up to  $800^\circ\text{C}$ . The CH<sub>4</sub> conversion ratio (%) were defined as  $100 \times (\text{mol CH}_{4,\text{in}} - \text{mol CH}_{4,\text{out}}) / \text{mol CH}_{4,\text{in}}$ . The apparent activation energy value was calculated from Arrhenius type plots ( $1,000/T$  vs. reaction rate) and obtained below 10% conversion of methane. The conversion ratio of CH<sub>4</sub> was detected by the  $m/z=15$  peak instead of the  $m/z=16$  peak (the major peak of methane) to avoid the interference caused by the fragmented carbon monoxide (0.9%), water (1.1%), carbon dioxide (8.5%) and oxygen (11%). All the tests were conducted with mass concentration determination (MCD) mode.

### Acknowledgements

Buğra Kayaalp thanks the MIN Graduate School International of for the financial support during his stay at KAIST. Kurt Klauke was financially supported by the PhD fellowship of the University of Hamburg. Prof. Roberto Scotti of the University Milano-Bicocca and Prof. Michael Fröba of the University of Hamburg are gratefully acknowledged for the support and the fruitful discussions. Andreas Kornowski of the University of Hamburg is gratefully acknowledged for electron microscopy

measurements. Siwon Lee, Jongsu Seo and WooChul Jung were financially supported by the Korea Institute of Energy Technology Evaluation and Planning (KETEP) and the Ministry of Trade, Industry & Energy (MOTIE) of the Republic of Korea (No. 20173010032120 and 20163030031850).

## Conflict of interest

The authors declare no conflict of interest.

**Keywords:** A-site deficiency · catalysis · flash sintering · oxygen exchange · surface reconstruction

- [1] Jennifer A. Dahl, A. Bettye L. S. Maddux, J. E. Hutchison, *Chem. Rev.* **2007**, *107*, 2228–2269.
- [2] M. L. Moreira, G. P. Mambriani, D. P. Volanti, E. R. Leite, M. O. Orlandi, P. S. Pizani, V. R. Mastelaro, C. O. Paiva-Santos, E. Longo, J. A. Varela, *Chem. Mater.* **2008**, *20*, 5381–5387.
- [3] I. Bilecka, M. Niederberger, *Nanoscale* **2010**, *2*, 1358.
- [4] S. Mascotto, O. Tsetsgee, K. Muller, C. Maccato, B. Smarsly, D. Brandhuber, E. Tondello, S. Gross, *J. Mater. Chem.* **2007**, *17*, 4387–4399.
- [5] O. Guillon, C. Elsässer, O. Gutfleisch, J. Janek, S. Korte-Kerzel, D. Raabe, C. A. Volkert, *Mater. Today* **2018**, *21*, 527–536.
- [6] G. Cerretti, M. Schrade, X. Song, B. Balke, H. Lu, T. Weidner, I. Lieberwirth, M. Panthöfer, T. Norby, W. Tremel, *J. Mater. Chem. A* **2017**, *5*, 9768–9774.
- [7] D. A. Molodov, N. Bozzolo, *Acta Mater.* **2010**, *58*, 3568–3581.
- [8] J. Cho, Q. Li, H. Wang, Z. Fan, J. Li, S. Xue, K. S. N. Vikrant, H. Wang, T. B. Holland, A. K. Mukherjee, *Nat. Commun.* **2018**, *9*, 1–9.
- [9] W. Rheinheimer, J. P. Parras, J. H. Preusker, R. A. De Souza, M. J. Hoffmann, *J. Am. Ceram. Soc.* **2018**, *0*–2.
- [10] M. Cologna, J. S. C. Francis, R. Raj, *J. Eur. Ceram. Soc.* **2011**, *31*, 2827–2837.
- [11] Y. Zhang, J. Nie, J. M. Chan, J. Luo, *Acta Mater.* **2017**, *125*, 465–475.
- [12] W. Ji, B. Parker, S. Falco, J. Y. Zhang, Z. Y. Fu, R. I. Todd, *J. Eur. Ceram. Soc.* **2017**, *37*, 2547–2551.
- [13] A. Karakuscu, M. Cologna, D. Yarotski, J. Won, J. S. C. Francis, R. Raj, B. P. Uberuaga, *J. Am. Ceram. Soc.* **2012**, *95*, 2531–2536.
- [14] A. Gaur, V. M. Sglavo, *J. Mater. Sci.* **2014**, *49*, 6321–6332.
- [15] J. Won, L. J. Vernon, A. Karakuscu, R. M. Dickerson, M. Cologna, R. Raj, Y. Wang, S. J. Yoo, S.-H. Lee, A. Misra, *J. Mater. Chem. A* **2013**, *1*, 9235.
- [16] P. Dolcet, S. Diodati, F. Zorzi, P. Voepel, C. Seitz, B. M. Smarsly, S. Mascotto, F. Nestola, S. Gross, *Green Chem.* **2018**, *26*, 2257–2268.
- [17] J. Hwang, R. R. Rao, L. Giordano, Y. Katayama, Y. Yu, Y. Shao-Horn, *Science* **2017**, *358*, 751–756.
- [18] F. Polo-Garzon, S. Z. Yang, V. Fung, G. S. Foo, E. E. Bickel, M. F. Chisholm, D. E. Jiang, Z. Wu, *Angew. Chem. Int. Ed.* **2017**, *56*, 9820–9824; *Angew. Chem.* **2017**, *129*, 9952–9956.
- [19] G. S. Foo, Z. D. Hood, Z. Wu, *ACS Catal.* **2018**, *8*, 555–565.
- [20] B. E. Kayaalp, Y. J. Lee, A. Kornowski, S. Gross, M. D'Arienzo, S. Mascotto, *RSC Adv.* **2016**, *6*, 90401–90409.
- [21] B. Kayaalp, S. Lee, K. Klauke, S. Jongsu, L. Nodari, A. Kornowski, W. Jung, S. Mascotto, *Appl. Catal. B* **2019**, *245*.
- [22] E. Mutoro, E. J. Crumlin, M. D. Biegalski, H. M. Christen, Y. Shao-Horn, *Energy Environ. Sci.* **2011**, *4*, 3689–3696.
- [23] S. F. Wagner, C. Warnke, W. Menesklou, C. Argiris, T. Damjanovi, G. Borchardt, E. Ivers-tiffée, *Solid State Ionics* **2006**, *177*, 1607–1612.
- [24] F. Polo-Garzon, V. Fung, X. Liu, Z. D. Hood, E. E. Bickel, L. Bai, H. Tian, G. S. Foo, M. Chi, D. Jiang, *ACS Catal.* **2018**, *8*, 10306–10315.
- [25] L. Bai, F. Polo-Garzon, Z. Bao, S. Luo, B. M. Moskowitz, H. Tian, Z. Wu, *ChemCatChem* **2019**, *11*, 2107–2117.
- [26] S. Ouyang, P. Li, H. Xu, H. Tong, L. Liu, J. Ye, *ACS Appl. Mater. Interfaces* **2014**, *6*, 22726–22732.
- [27] S. Brunauer, P. H. Emmett, E. Teller, *J. Am. Chem. Soc.* **1938**, *60*, 309–319.
- [28] M. Biesuz, V. M. Sglavo, *J. Eur. Ceram. Soc.* **2019**, *39*, 115–143.
- [29] B. Koo, K. Kim, J. K. Kim, H. Kwon, J. W. Han, W. Jung, *Joule* **2018**, *2*, 1476–1499.
- [30] B. Koo, H. Kwon, Y. Kim, H. G. Seo, J. W. Han, W. Jung, *Energy Environ. Sci.* **2018**, *11*, 71–77.
- [31] R. Meyer, R. Waser, J. Helmbold, G. Borchardt, *J. Electroceram.* **2002**, *9*, 101–110.
- [32] F. A. Kröger, H. J. Vink, *Solid State Phys.* **1956**, *3*, 307–435.
- [33] M. J. Akhtar, Z.-U.-N. Akhtar, R. A. Jackson, C. R. A. Catlow, *J. Am. Ceram. Soc.* **1995**, *78*, 421–428.
- [34] K. Gömann, G. Borchardt, M. Schulz, A. Gömann, W. Maus-Friedrichs, B. Lesage, O. Kaitasov, S. Hoffmann-Eifert, T. Schnell, *Phys. Chem. Chem. Phys.* **2005**, *7*, 2053–2060.
- [35] R. Chaim, G. Chevallier, A. Weibel, C. Estournès, *J. Appl. Phys.* **2017**, *121*, 145103.
- [36] K. S. Naik, V. M. Sglavo, R. Raj, *J. Eur. Ceram. Soc.* **2014**, *34*, 4063–4067.
- [37] J. Narayan, *Scr. Mater.* **2013**, *69*, 107–111.
- [38] Y. Zhu, W. Zhou, J. Yu, Y. Chen, M. Liu, Z. Shao, *Chem. Mater.* **2016**, *28*, 1691–1697.
- [39] N. A. Merino, B. P. Barbero, P. Eloy, L. E. Cadús, *Appl. Surf. Sci.* **2006**, *253*, 1489–1493.
- [40] J. Zhu, H. Li, L. Zhong, P. Xiao, X. Xu, X. Yang, Z. Zhao, J. Li, *ACS Catal.* **2014**, *4*, 2917–2940.
- [41] I. Bykov, M. Makarova, V. Trepakov, A. Dejneka, L. Yurchenko, *Phys. Status Solidi* **2013**, *824*, 821–824.
- [42] S. Ahuja, T. R. N. Kutty, *J. Photochem. Photobiol. A* **1996**, *97*, 99–107.
- [43] C. Oliva, L. Bonoldi, S. Cappelli, L. Fabbrini, I. Rossetti, L. Forni, *J. Mol. Catal. A Chem.* **2005**, *226*, 33–40.
- [44] W. L. Harrigan, S. E. Michaud, K. A. Lehuta, K. R. Kittilstved, *Chem. Mater.* **2016**, *28*, 430–433.
- [45] R. a. De Souza, *Adv. Funct. Mater.* **2015**, *25*, 62326–6342.
- [46] R. A. De Souza, *Phys. Chem. Chem. Phys.* **2009**, *11*, 3010.
- [47] P. Lupetin, G. Gregori, J. Maier, *Angew. Chem. Int. Ed.* **2010**, *49*, 10123–10126; *Angew. Chem.* **2010**, *122*, 10321–10324.
- [48] G. Gregori, S. Heinze, P. Lupetin, H. U. Habermeier, J. Maier, *J. Mater. Sci.* **2013**, *48*, 2790–2796.
- [49] P. Balaya, J. Jamnik, J. Fleig, J. Maier, *Appl. Phys. Lett.* **2006**, *88*, 062109.
- [50] Y. Chen, W. Jung, Z. Cai, J. J. Kim, H. L. Tuller, B. Yildiz, *Energy Environ. Sci.* **2012**, *5*, 7979–7988.
- [51] W. Jung, H. L. Tuller, *Energy Environ. Sci.* **2012**, *5*, 5370–5378.
- [52] Y. Li, W. Zhang, Y. Zheng, J. Chen, B. Yu, Y. Chen, M. Liu, *Chem. Soc. Rev.* **2017**, *46*, 6345–6378.
- [53] F. S. Baumann, J. Fleig, M. Konuma, U. Starke, H.-U. Habermeier, J. Maier, *J. Electrochem. Soc.* **2005**, *152*, A2074.
- [54] G. J. la O', R. F. Savinell, Y. Shao-Horn, *J. Electrochem. Soc.* **2009**, *156*, B771.
- [55] E. Y. Konyshva, X. Xu, J. T. S. Irvine, *Adv. Mater.* **2012**, *24*, 528–532.
- [56] G. Tsekouras, J. T. S. Irvine, *J. Mater. Chem.* **2011**, *21*, 9367.
- [57] M. C. Verbraeken, T. Ramos, K. Agersted, Q. Ma, C. D. Savaniu, B. R. Sudiredy, J. T. S. Irvine, P. Holtappels, F. Tietz, *RSC Adv.* **2015**, *5*, 1168–1180.
- [58] K. Aika, J. H. Lunsford, *J. Phys. Chem.* **1977**, *81*, 1393–1398.
- [59] C. Oliva, L. Bonoldi, S. Cappelli, L. Fabbrini, I. Rossetti, L. Forni, *J. Mol. Catal. A Chem.* **2005**, *226*, 33–40.
- [60] M. Iwamoto, J. H. Lunsford, *J. Phys. Chem.* **1980**, *84*, 3079–3084.
- [61] Y. Takita, J. H. Lunsford, *J. Phys. Chem.* **1979**, *83*, 683–688.
- [62] M. Che, A. J. Tench, *Adv. Catal.* **1983**, *32*, 1–148.

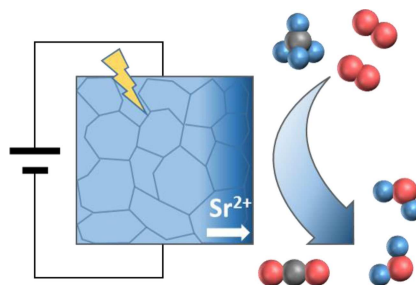
Manuscript received: May 27, 2019

Revised manuscript received: May 6, 2019

Version of record online: ■■■, ■■■■

## FULL PAPER

**Strontium titanate nanoparticles** prepared by hydrothermal synthesis were exposed to conventional and electric field assisted consolidation under air. Application of an electric field reduced grain growth and resulted in an enhanced segregation of strontium to the surface. The modification of the surface chemistry of the materials engendered significant improvement of the catalytic full oxidation of methane with respect to the conventionally treated counterpart



*K. Klauke, Dr. B. Kayaalp, Dr. M. Biesuz, Dr. A. Iannaci, Prof. Dr. V. M. Sglavo, Prof. Dr. M. D'Arienzo, S. Lee, J. Seo, Prof. Dr. W. Jung, Prof. Dr. S. Mascotto\**

1 – 10

**Enhancement of the SrTiO<sub>3</sub> Surface Reactivity by Exposure to Electric Fields**

